



## **Effect of high-energy laser welding parameters on the microstructure and mechanical properties of 304 stainless steel**

### **304 Paslanmaz çeliğin mikroyapı ve mekanik özellikleri üzerinde yüksek enerjili lazer kaynak parametrelerinin etkisi**

**Simge Gençalp İrizalp<sup>1\*</sup>**, **Burçak Kardelen Köroğlu<sup>1</sup>**

<sup>1</sup> Manisa Celal Bayar Üniversitesi Mühendislik Fakültesi Makina Mühendisliği Bölümü, Manisa, TÜRKİYE  
Sorumlu Yazar / Corresponding Author \*: [simge.gencalp@cbu.edu.tr](mailto:simge.gencalp@cbu.edu.tr)

Geliş Tarihi / Received: 25.04.2020

Kabul Tarihi / Accepted: 10.06.2020

*Atıf şekli/How to cite:* GENÇALP İRİZALP, S., KÖROĞLU, B.K. (2021). Effect of high-energy laser welding parameters on the microstructure and mechanical properties of 304 stainless steel. DEUFMD, 23(67), 179-194.

Araştırma Makalesi/Research Article

DOI:10.21205/deufmd.2021236716

#### **Abstract**

Autogenous bead-on-plate laser welding was performed on 2 mm 304SS materials at different heat inputs. The influence of laser energy in low welding speeds on weld performance using a Nd:YAG laser was studied. The weld performance was characterized in terms of weld bead morphology, microstructure and mechanical properties. The result revealed that the crater increased with the increase of heat input, so there is a linear relationship between crater and heat input. The gradual increase of the heat input was not directly related to the penetration of the weld bead. At the highest heat input, weld beads considerably expanded and also the crater deepened, the hardness increased in these joints while tensile strength and ductility reduced. The best mechanical properties were obtained with high laser energy at intermediate heat input. These weldments exhibited better strength even better than base metal 304SS. The microhardness values were distributed homogeneously from the fusion zone to the base metal. Laser energy increased the ferrite network and brought finer ferrites. As a result, usable laser welding parameters in terms of good strength, as well as good ductility and weld bead morphology were defined for welding 304 SS with 2 mm thickness.

**Keywords:** Laser welding 1, Mechanical properties 2, Microstructure 3, 304 Stainless steel 4

#### **Öz**

2 mm kalınlığında 304SS malzemelerine otojen plaka üstü dikiş şeklinde farklı ısı girdilerine sahip lazer kaynağı uygulanmıştır. Nd: YAG lazer kullanılarak özellikle düşük kaynak hızlarında lazer enerjisinin kaynak performansı üzerine etkisi araştırılmıştır. Kaynak performansı kaynak dikiş morfolojisi, mikroyapı ve mekanik özellikler açısından karakterize edilmiştir. Sonuçlar, ısı girdisinin artmasıyla kraterin arttığını ortaya koymuş, bu nedenle krater ve ısı girdisi arasında doğrusal bir ilişki olduğu belirtilmiştir. Isı girdisindeki kademeli artışın kaynak dikişinin penetrasyonu ile doğrudan ilişkili olmadığı bulunmuştur. En yüksek ısı girdisinde, kaynak dikişleri önemli ölçüde genişlemiş ve krater derinleşmiştir, bu kaynak dikişlerinin sertliği artarken çekme dayanımı ve süneklik azalmıştır. En iyi mekanik özellikler orta seviyedeki ısı girdisine sahip yüksek lazer enerjisi ile elde edilmiştir. Bu

kaynaklar, 304SS ana metalinden daha iyi mukavemet sergilemiştir. Mikrosertlik değerleri füzyon bölgesinden ana metale homojen olarak dağılmıştır. Lazer enerjisi ferrit ağını arttırmış ve daha ince ferritler oluşturmuştur. Sonuç olarak bu çalışma ile 304 SS 2 mm kalınlığındaki plakaların kaynağında iyi mukavemet, iyi süneklik ve kaynak dikiş morfolojisi açısından kullanılabilir lazer kaynak parametreleri tanımlanmıştır.

**Anahtar Kelimeler:** Lazer Kaynak 1, Mekanik Özellikler 2, Mikroyapı 3, 304 Paslanmaz çelik 4

## 1. Introduction

High-energy welding processes are applied in a range of industrial applications due to the narrow heat-affected zone (HAZ), low residual strains, uniform grain structure, high productivity and low operating costs compared to conventional welding processes [1]. Laser welding is a high-energy density welding process [2]. Deep penetration can be easily produced using high-energy laser welding. The most important factor affecting the depth of penetration was found to be the distribution of the incident energy flux [3]. Short-time interval energy inputs result in a minimized thermal loading of the based material owing to the pulsed high-energy laser welding [4]. The laser welding contains a number of beneficial characteristics, such as low distortion, noncontact process, suitability to automation, controllability, repeatability, high efficiency, local applicability, the possibility of welding without filler metal [5]. Laser welding also has a number of disadvantages. Microstructural defects in the laser welded structure may be present. These can be pores, cracks, presence of  $\delta$ -ferrites, coarse columnar morphology. Especially, the formation of pores and cracks is very easy. The parameters of laser welding directly affect the weld bead quality. Optimization of a good weld bead geometry is achieved with parameters such as laser power, welding speed, pulse duration, shielding gas. However, optimizing weld bead geometry may not result in an excellent performance. It is very important to develop mechanical properties besides well welding geometry since the mechanical properties are closely related to grain structure and distribution of phases.

Austenitic stainless steel is in a very important material category due to its superior material properties and is preferred in a wide range of industrial applications [6]. 304 stainless steel (304 SS) is one of the most widely use austenitic stainless steel and it has been preferred in a

variety of applications including nuclear reactor components, aircraft fittings, aerospace components, vessel internals and valve bodies due to its special properties such as good corrosion, toughness, ductility and easy fabrication [2,7,8]. The key components such as the welded joints in nuclear power plants, design and structural integrity are required to have good mechanical properties. The welding process produces the weakness in mechanical properties due to changing microstructure which happens because of heating and cooling steps. As a result of slow cooling due to the high heat input in conventional arc welding methods, coarse grain structure develops in large HAZ. The chromium carbides deposited at the grain boundaries weaken the mechanical properties of the stainless steel joints [7]. 304 SS is frequently welded in many industrial fields and the laser welding of this material is often of interest. There are some reports concerning the laser welding of austenitic stainless steels. Mao et al. [9] examined the microstructure-property relationship of laser welded AISI 304/308L SS. They performed the nanoscale characterization by evaluating grain boundary size and orientation. Shah et al. [10] analyzed the melting and solidification behavior during spot laser welding of 304 SS. They evaluated heat transport phenomena related to the melting and solidification stage by taking into consideration the computational model. The heat transfer and fluid flow during solidification determine the microstructure of the weld zone, thereby affecting both its physical and metallurgical properties. The pulsed Nd:YAG laser welding of 304 and 316 SS was investigated by Kumar et al. [2] using DOE/analysis of variance approach. They found that laser welded 304 SS had better mechanical properties than laser welded 316 SS. They performed the welds in low peak power and high welding speeds. Geng et al. [11] carried out dissimilar pulsed laser welding of AISI 304 and 420 SS. They researched the effect of laser parameters on the mechanical and

microstructural properties of the joints. They reported that more laser beam energy or power density notably changed the austenitic fusion zone temperature distribution. The peak temperature changed the grain morphology. The microstructure of the fusion zone composed of coarse acicular ferrite and grain boundary ferrite structure in all the weldments.

In general, an austenitic stainless steel weld zone includes  $\delta$ -ferrite and austenite. In terms of mechanical properties, the role of  $\delta$ -ferrite phase is important. For example, the amount of  $\delta$ -ferrite generally ranges from 3% to 8% to prevent solidification cracking. Non-equilibrium rapid solidification during laser welding leads to incomplete  $\delta$ - $\gamma$  transformations, resulting in metastable  $\delta$ -Fe phases and the heat input during the process greatly affects the  $\delta/\gamma$  ratio in the fusion zone [2]. The presence of unstable  $\delta$ -ferrite in austenitic stainless steels disrupts ductility and causes the initiation and propagation of cracks at the  $\gamma/\delta$  interface [12].

304 SS is commonly used in many industrial applications in the as-welded condition and this paper focuses on laser welding of 304 SS without filler metal. Besides that weld bead appearance is important in the welded constructions, their mechanical properties play a central role especially in load-bearing systems. A few previous studies in the literature concentrated on the relationship microstructure and mechanical performance of laser welded 304 SS [2,9,13-17]. High-energy laser welding in 304 SS material has been rarely reported [2,13,18,19]. High power density permits deep welding and produces narrow HAZ and fine grain structure and minimal distortion by restricting the amount of energy emitted to the material to allow transition from conduction mode to keyhole mode [20]. When a Gaussian representation of heat source during laser irradiation is considered, only the heat input on the top of the workpiece may not lead to accurate results. Especially for high-energy laser beam, the increase in peak power results in rapid penetration through the thickness of the material. Laser properties, thermal conductivity, base metal melting point and laser-material absorption are determinative in terms of metallurgical and mechanical properties of the weld zone [2]. 304 SS has a high absorption of the laser beam. The weld bead performance of stainless steel is increased by high-energy laser

[18]. In this study, microstructure and mechanical properties of 304 SS joints after high-energy laser welding were investigated. The goal of this study was to evaluate changes of mechanical properties, on the characteristics of the weld bead, such as the crater and penetration as well as grain morphology and tendency to form a crack. This work revealed a good cause-effect relationship about the effects of pulsed laser welding parameters on the mechanical properties of the welded joints of austenitic stainless steel. Weld bead geometry, microstructure, microhardness, residual stress distribution and tensile mechanical properties of welded joints were examined and compared with non-welded 304 SS. In addition, the reasons behind obtaining better mechanical properties than non-welded 304 SS material were examined.

## 2. Material and Method

2 mm thick AISI 304 materials were used as the base metal for the welding process. The chemical compositions of the base metal are shown in Table 1. Fine austenitic structure, annealing twins and a little delta ferrite stringers are seen in the microstructure of as-received material (Figure 1).

**Table 1.** Chemical composition of AISI 304 stainless steel

C	Si	Mn	P	S	Cr	Ni	Fe
0.08	0.75	2.00	0.045	0.030	18-	8-	Bal.
					20	10.5	

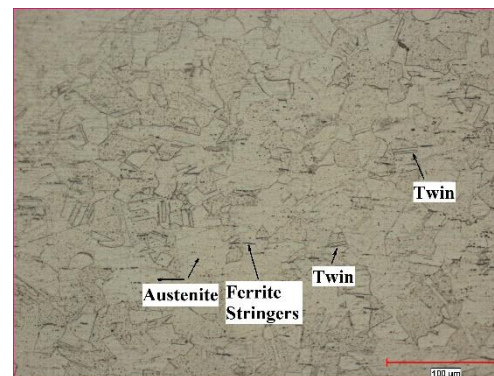


**Figure 1.** The microstructure of 304 SS base metal

Welding was performed using a pulsed Nd:YAG laser machine, WF300 model with 30J max. laser pulse energy with a continuous wavelength of 1064 nm. The laser head was equipped with a focal length of 200 mm providing a laser spot size of 0.6 mm at the focal point. Argon gases were used as shielding gases with a flow rate of 20 lpm. Samples were cut from the 1000x1250x2 mm sheets by laser cutting machine prior to welding with reference to ASTM-E8/E8M standard. However, before welding, a tolerance was left in cut samples with 2 mm for trimming. After welding, all samples were trimmed into test specimen dimensions by machining and the final sample dimensions are given in Figure 2. The laser welding was carried out as an autogenous bead on the plate. Maximum penetration depth, as well as a minimum crater, represents the welding quality in terms of weld bead geometry. Here the aim is to investigate the welding parameters to observe weldability in terms of weld bead geometry. The laser welding process parameters were determined regarding maximum penetration and considering that they are in a relationship with each other are given in Table 2. The very high average power of the laser machines (near the maximum average power) can be problematic because high frequency values result in high a wattage and the maximum peak power of this machine is 6 kW. In high powers, it is suitable to work with low frequency or pulse energy. Extending the pulse duration and slightly increasing the peak power without increasing too high for the frequency have been considered to increase the penetration depth and to achieve optimum welding parameters.

The laser welds were manufactured at different welding speeds, peak power and pulse duration which represented in Table 2. The welded samples were sectioned and prepared metallographically. And then, the polished samples were etched with 10 ml HCl, 15 ml HNO<sub>3</sub>, 10 ml acetic acid and 2-3 drops of glycerine. The microstructures on the weld bead cross section were observed by stereo microscope (SM) and the microstructure of fusion zone (FZ), heat affected zone (HAZ) and base metal (BM) were examined by optical microscope (OM) Nikon Eclipse LV150N. The Vickers hardness were performed at a load of 10g with a holding time 10s on the longitudinal section at the upper, middle and bottom part and the microhardness measurement lines (face, middle and root) are shown in Figure 3.

**Table 2.** Laser welding parameters

Weld number	Peak power (kW)	Welding speed (cm/min)	Pulse duration (ms)	Frequency (Hz)	Laser pulse energy (J)
Type 1	2.7	1	10	13.5	27
Type 2	2.5	1	10	14.5	25
Type 3	2.5	1	7	17.7	17.5
Type 4	2.7	1	7	16.4	18.9
Type 5	2.7	2	10	13.5	27
Type 6	2.5	2	10	14.5	25
Type 7	2.7	2	7	16.4	18.9
Type 8	2.5	2	7	17.7	17.5

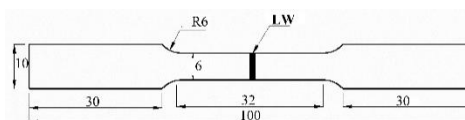


**Figure 2.** Dimensions of the tensile test specimens used in the present study

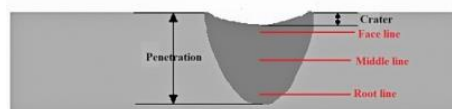


**Figure 3.** Schematic of the microhardness measurement lines on the weld bead cross-section

Tensile tests were carried out at a constant cross-head speed of 4 mm/min at room temperature on a Shimadzu Autograph 100kN testing machine. The elongation of the samples was measured with video-extensometer (Shimadzu Noncontact Video Extensometer DVE-101/201), with trapezium (advanced software for materials testing) for machine control and data acquisition. Six tensile test specimens were prepared for full penetration joints. The investigations on mechanical properties have been performed only in joints where full penetration had happened. Thus, the effects of crater and width on mechanical properties were investigated in welded joints. Residual stress analysis has been carried out on GE-Seifert XRD. The X-ray source was Cr-K $\alpha$  and the experiments were performed on (220) diffraction lattice plane. Bragg angle was 128.78°. The residual stresses obtained on the surface based on the distance away from the weld bead were measured.

### 3. Results and Discussion

Morphological examinations of all welds obtained from the parameters were given in

Figure 4. A crater formed on the joint in all parameters. It was obvious that the penetration varied according to the welding parameters. The obtained welds presented the transition from conduction to keyhole welding mode. Depending on the laser welding parameters, the heat conduction around the keyhole has changed and the weld bead has been affected. Wang et al. [21] joined dual phase steel by laser welding and used metaphors for bead morphology such as "cup cone" and "hour glass". In our study, Type 2, 3, 6 and 7 appear in the form of "cup cone", 3 and 5 appear in the form of "hour glass". Type 1 and 6 showed mainly excessive melting. Table 3 summarizes some results of laser welding. A relationship was established between crater and heat input and the graph was given in Figure 5. The crater increased as heat input increased. The increased energy transfer during welding will be increased the amount of material evaporated in the weld pool, thus material loss increases. And this will result in a larger crater [22]. It is known that low welding speed increases the penetration [5], as the speed increases, penetration depth changed from full penetration to partial penetration mode [23]. Low welding speeds have already been used (1 cm/min and 2 cm/min) in this study. If the weld bead width was evaluated, both the heat input and the power density became effective. In the welding regime where high heat input was applied, the heat conduction around the keyhole became more dominant and it extended the weld bead. The rise of the heat input partially affected the depth of the FZ and caused it to expand laterally. As the heat conduction increases, the weld bead begins to modify its circumference. Even a slight increase in peak power for similar heat input values increased the penetration depth, as seen in Type 1-Type 2 and Type 3-Type 4 and Type 5-Type 6. At low welding speed, the melted metal can have very enough time to flow and spread deeply in relatively high peak power levels and also there is also sufficient time for the rising of weld pool temperature. At overlarge speeds, the molten weld pool quickly solidifies and is also cooled down by the remaining BM portion without penetration [24]. Keeping the peak power at relatively high levels ensures that the laser energy increases. The high power density permits the welding based on the keyhole principle (deep penetration and narrow weld bead width), in this case, the reduced energy transferred to the material brings a narrow HAZ

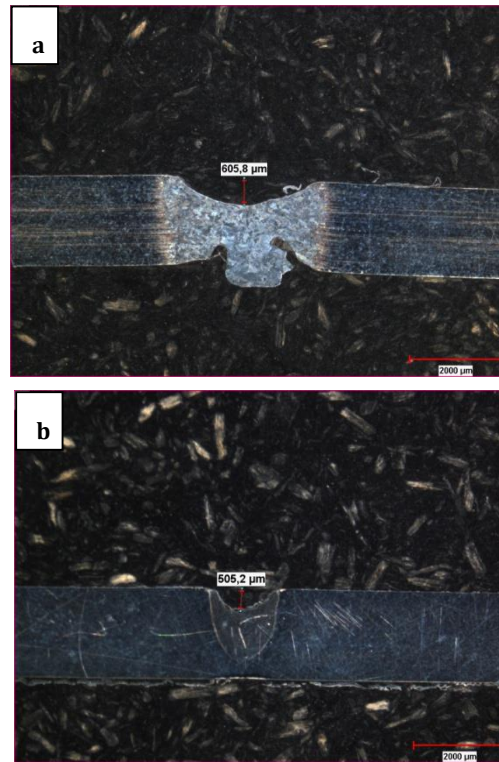
and low residual stress and distortion [2]. Following these inferences, a weld was performed except for the parameters in Table 2, where the heat input was low but the peak power was high. The goal of this weld was to make the crater even more minimal without losing penetration. The parameters for this welding were as follows: peak power was 3 kW, welding speed was 4 mm/s, pulse duration was 7 ms, and heat input was 463.72 J/mm.

**Table 3.** Results of laser welds

Weld number	Heat Input (J/mm)	Crater (mm)	Penetration (mm)
Type 1	2195.78	605.8	FP
Type 2	2183.73	505.2	LP
Type 3	1865.96	316.2	LP
Type 4	1867.22	359.3	FP
Type 5	1094.59	239.5	FP
Type 6	1088.58	213.3	LP
Type 7	930.81	174	LP
Type 8	930.18	188.5	FP

\*Full penetration (FP) and Lack of penetration (LW)

\*\*Heat Input (J/mm) = [Pulse energy (J) x Frequency (Hz)] / Welding speed (mm/s)



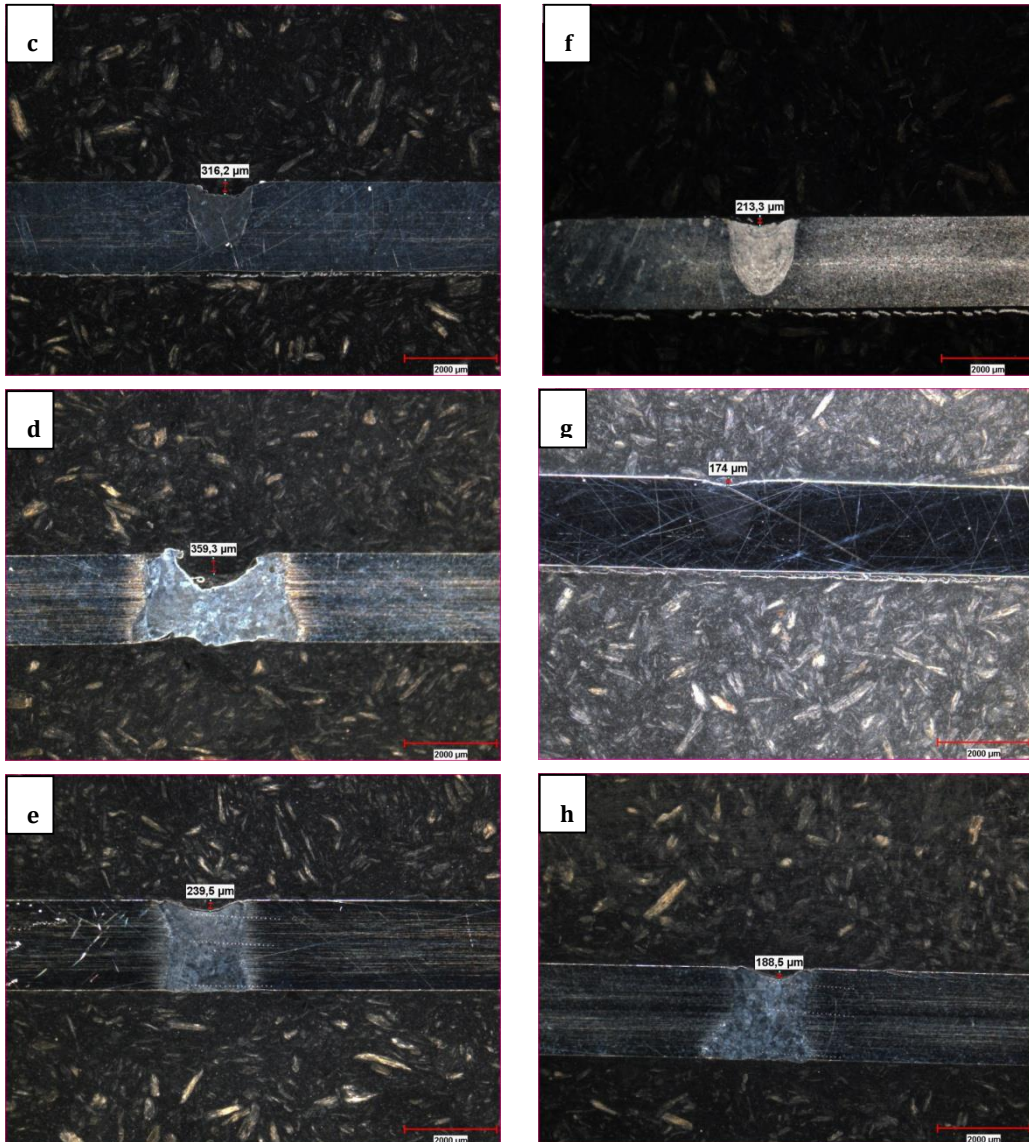


**Figure 4.** Macrostructure of the laser welded 304 samples, (a) Type 1, (b) Type 2, (c) Type 3, (d) Type 4, (e) Type 5, (f) Type 6, (g) Type 7, (h) Type 8

The weld obtained with these parameters was referred to as Type 9. Figure 6 showed the weld bead morphology obtained from the metallographic examination. The weld bead was obtained in which no crater was formed and full penetration was achieved. So, in this work, the lowest heat input of 463.72 J/mm and the highest heat input of 2195.78 J/mm obtained the

full penetration in the weldment. Since the very high heat inputs increase the heat conduction, it triggers the crater formation. As foreseen, crater-free bead was obtained due to low heat input, and full penetration was achieved with increasing the peak power. The reason why the welding speed is partially increased for Type 9 is to reduce the heat input, so that heat conduction

around the weld pool is not predominant. However, there was a crack in this weld bead. The crack formation is discussed in detail below.

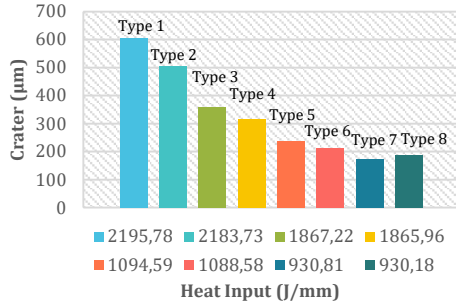


**Figure 5.** Effect of heat input on the crater formation

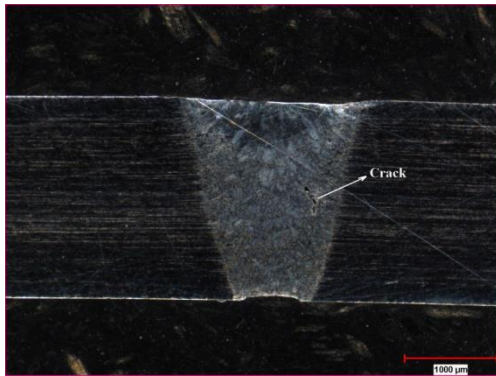


**Figure 6.** Macrostructure of Type 9

Satisfactory joints were achieved in Type 5, Type 8 and Type 9, regarding the full penetration, narrow bead, minimum crater. Type 1 and 4 welds took place resulting in considerable crater formed along with full penetration. The laser welded joints achieved the full penetration were exposed to the tensile tests as well as as-received (no-welded) 304 SS. The results including the average of 6 tensile tests were presented in Table 4. A higher tensile strength value (513.4 MPa) and the largest ductility (35%) were obtained in Type 8. While Type 9 was so good in terms of weld bead morphology, tensile strength value was 460 MPa as the value was definitely not the best strength. Since Type 9 included a crack, the strength was relatively low although it had a narrow and flat weld bead. The strength of the as-received (no-welded) material was 477 MPa and, as shown, the strength of the welded joint made with the Type 5 laser welding parameters was higher than no-welded 304 SS.

The lowest strength was obtained in Type 1. This value was 167 MPa and extremely low. For the same welded joints, the ductility decreased to 5%. Both the strength and ductility of the over-melted and expanded weld bead decreased with the high heat input and high laser pulse energy. Type 4 also showed relatively low strength, which was associated with a large weld bead and crater. Table 5 indicated the residual stress values on the weld zone and HAZ for Type 5 welding. As-received 304 SS exhibits mainly compressive in nature depending on manufacturing history (hot rolling). It is also reported that residual stress in FZ and HAZ is tensile in nature. The increase in residual stress from compressive type to tensile type is due to the thermal effect in the weld zone. This increase is expected after welding. The increase in energy during welding leads to an increase in residual tensile stress [25]. Type 5's mechanical properties not deteriorating may also be attributed to the slight increase in residual stress. High value of residual stress was concentrated in HAZ because of the relatively slow cooling rates. Moreover, the phase change during cooling due to expansion resulted in high residual stress value in HAZ [26].

Figure 7 and 10 showed microstructural morphology of full penetrated welds in high magnifications. According to the microstructures, the grain growth was different at various locations of the weld. With an increased cooling rate, further incomplete conversion of weld metal results in the formation of retained-delta ferrite [27]. High cooling rates during welding partially suppressed the austenite transformation of delta-ferrite. The microstructure was therefore different very from that of the BM (Figure 1).

**Table 4.** Tensile properties for the conditions of full penetrated workpieces

Weld number	Tensile Strength (MPa)	Elongation (%)
Type 8	480.8	31.45
Type 4	360.8	8.46
Type 1	167	6.85
Type 5	513.4	34.97
Type 9	460	28.65
As-received (no-welded)	477.3	58

**Table 5.** Residual stresses of as-received material and Type 5 laser welded material

304 SS (as-received)	FZ	HAZ
$-99.9 \pm 68.9$ MPa	$125.9 \pm 53.7$ MPa	$188.3 \pm 63.6$ MPa

Since different laser parameters change the melting and solidification rates of the material, in particular, the delta ferrite changes in content and shape. In this study, skeletal delta-ferrite and lathy delta ferrite morphology were generally observed in weld zones. Balajaddeh et. al. [28] and Bilmes et al. [29] have been reported that the simultaneous occurrence of these morphologies in the weld metal is due to local changes in cooling rates and chemical compositions. During cooling after welding, the melted metal solidified first to delta ferrite in the form columnar dendrite, which then happened solid-state transformation to austenite. Delta ferrite indicated by the white arrow in Figure 7. Austenite in the form equiaxed dendrite grew on the whole Type 4 weld zone. Moreover, in high magnification, carbide structure was observed in FZ. It has a fine but localized carbide structure. The carbide precipitates were not found in other weldments. Chromium carbides accumulated in grain boundaries weaken the mechanical properties of stainless steel joints [7]. As the weldment cools to ambient temperature, some carbide precipitation segregation can be revealed as a result of the slow cooling rates. [30].

At Type 9, when the peak power was high, FZ continued to absorb the laser energy. The temperature difference between FZ and BM rises and as a result of rapid cooling, the columnar grains grow all over FZ (including face and root) and tend to form cracks. The microstructures of face, middle and root regions were given in Figure 8. When the temperature difference between FZ and BM is high, the temperature gradient and the cooling rate will be high. It is known that during the solidification if the temperature gradient is high, the columnar grains will grow. As a result, columnar grains formed at the beginning of solidification [31].

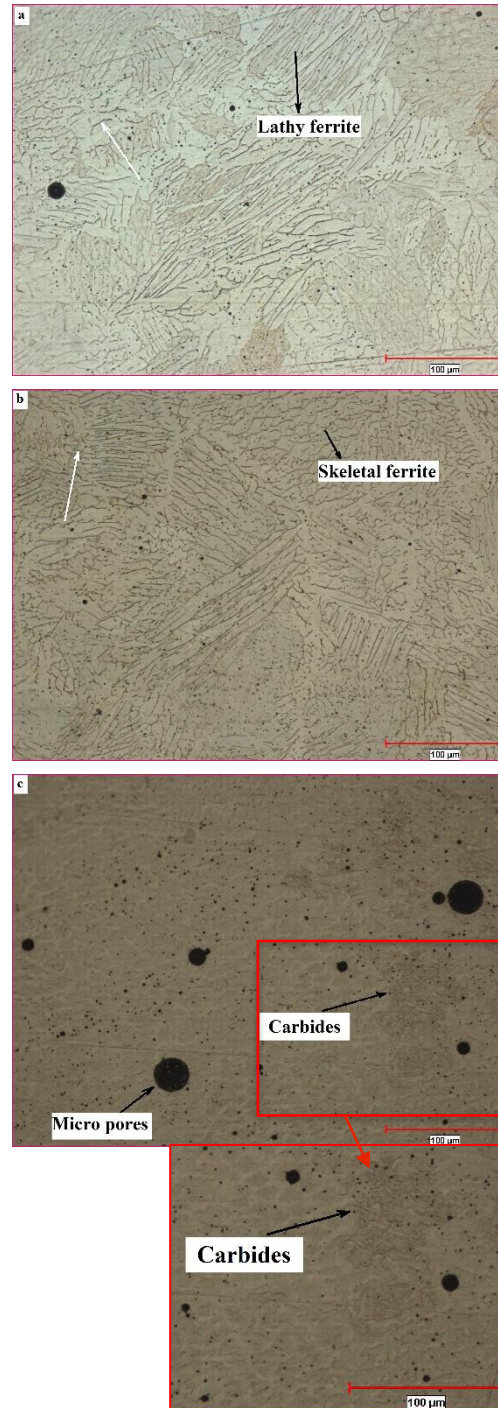




**Figure 7.** The fusion zone microstructures in high magnifications of (a) Type 8, (b) Type 4, (c) Type 1 and (d) Type 5

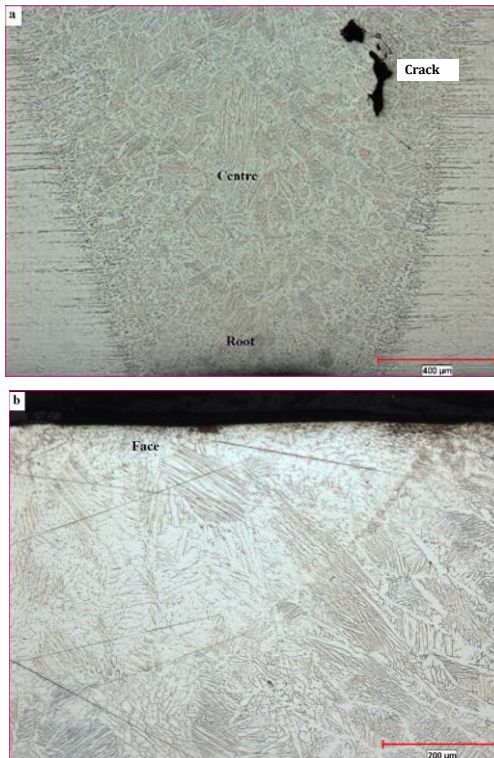


**Figure 8.** The weld metal of Type 8 containing middle and root regions (a), face in high magnification (b)

Accordingly, it was clear that columnar growth was dominant in the whole weld. Nucleation is low due to low heat input and high welding speed [32]. As can be also seen from Figure 6, the crystals grew more linearly and collided towards the upper center of the weld bead. The thermal

stresses of the weld are tensile type, and after pulsed laser radiation, thermal and shrinkage contraction begins in the FZ, simultaneously spreading heat to the BM and leading to expansion. This results in tensile strain in the weld zone [33]. The crack initiation and propagation are also easier in the coarse columnar zone. According to the shrinkage-brittleness theory, the contraction strains increase from coherent temperature to solid temperature during cooling [34]. In this critical temperature range, the remaining liquid phase cannot move freely due to the presence of the solid phase network. Consequently, the liquid phase cannot flow freely between the dendrites and thus also can not backfill the dendrite shrinkage. The crack is initiated and also frequently propagated along the grain boundaries [33]. There was a coarser grain growth in the FZ microstructures of Type 9. With the increase in peak power, the total energy stored by the weld zone increases during laser radiation, and so enthalpy increases [35]. Therefore, melt pool depth increased in this weldment. When Type 1 and Type 5 were compared, increasing the welding speed from 1 to 2 cm/min at the same peak power value (2.7 kW) increased the nucleation according to the microstructures. The mechanical properties (strength, toughness, etc.) of Type 5, which had a narrow and deep welded metal, improved [32]. In this case, unlike in Type 9, the possibility of solidification cracking reduced.

Considering Type 4, the pulse energy was relatively low, the FZ absorbed less energy during pulsed radiation. Furthermore, in this condition, the pulse duration was short, i.e. the time a laser pulse interacted with the material was short. The temperature difference between FZ and BM is reduced, thus cooling is relatively slow. The grains were mostly equiaxial and cellular due to decreasing temperature gradient and in particular, the FZ microstructure exhibited skeletal delta-ferrite in austenite matrix (Figure 9). In cases where the laser energy is not high, the temperature gradient is expected to decrease as solidification continues. Decreasing the temperature gradient results in equiaxed dendrite formation [31]. The dense amount of pores was also noteworthy. Although equiaxial grain growth was positive in terms of toughness, the formation of numerous pores and large craters weakened the mechanical properties. A unique feature of keyhole mode

laser welding (deep penetrated) is a large bubble formation. The formation of large pores is inhibited by stabilizing the keyhole. This is achieved by pulse effect during laser radiation by imposing forced oscillation of the keyhole [36, 37]. Figure 7b divulged the presence of micro pores, moreover, Figure 9 illustrated the denser pore structure of the Type 4 weld. The largest pores were formed in Type 4, they were approximately 30  $\mu\text{m}$  and that known as micro pores. The pores were not localized and they were observed at the face, middle and root of the weld. The inner surface of the porosities was seen smooth. It was clear that the pore diameters due to excessive melting and broadening increased. Moreover, in this study, very fine and more evenly distributed pores have generally occurred in other full-penetrated welds (the pore size decreased to less than 10  $\mu\text{m}$ ). Low welding speeds allow gas to nucleate and grow into small bubbles [38].

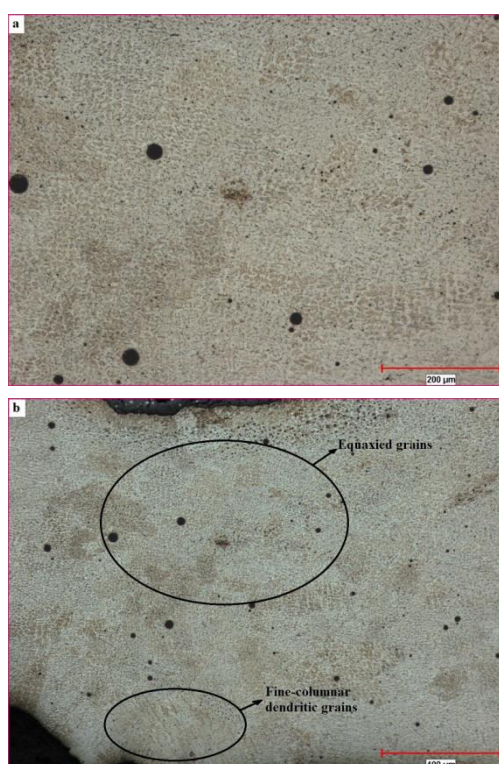


**Figure 9.** Type 4 welding microstructure (a) middle of the fusion zone in high magnification and (b) whole weld zone

As is known, HAZ microstructure significantly affects the mechanical properties of welded

materials. The HAZ width is also especially critical. In the HAZ, the grain size increases with heat input as well as a wider zone [39-41]. The HAZ width was narrowed by the reduction of heat input (Figure 10). Vermicular ferrite structure was observed partly. The HAZ is generally formed in a coarse-grained morphology, and both the mechanical and corrosion properties of this zone can be often different from the BM and FZ. The narrowing of HAZ positively affects the mechanical properties of the joints. It is known that austenitic stainless steels have low thermal conductivity [42]. The low thermal conductivity causes heat to be localized so that the localized heat is conducted slowly through the bulk metal while the laser beam moves at a given welding speed, which increases both the HAZ and the grain size [43]. In this study, it was noteworthy that HAZ was very narrow particularly in intermediate heat input conditions which had full penetration (Type 5 and 8). The largest HAZ was obtained in Type 1. It was the parameter that the lowest mechanical properties were obtained. This is related to the high heat input. HAZ generally spends a longer time at peak temperatures during the high heat input welds compared to the low heat input welds [44]. While the narrow HAZ and FZ are associated with low heat input, increasing the peak power which increases the penetration depth, may also trigger weld cracks. Although welding bead morphology looked good in Type 9 welding, mechanical properties were weakened due to undesirable tensile strains.

The grain size difference of Type 1 and 9 welds which had the lowest and highest heat inputs was very clear in Figure 10 and the weld zone of Type 1 was really fine-grained. In the literature, it is clear that high heat input creates a widely spaced ferrite network with relatively low cooling rates and coarse grain structure, and lower heat inputs bring a finer grain morphology and thus form a finer ferrite network. However, in high energy beam processes, ferrite morphology may go beyond traditional expectation, since solidification already occurs very quickly in a small area during laser welding. In this case, cooling rates become very sensitive to power density, pulse energy and welding speed. The effect of process parameters on the solidification behavior can be interesting. During pulsed laser welding, the pulsing affects the metallurgical properties of the weldment. Increasing laser energy, especially at low speeds,

increases the thermal effect with successive laser pulses, and so the overall temperature of the weld metal increases. Weld metal may remain molten even if the laser pulse is switched off [45]. The peak temperature of the weld metal and the cooling rate at each location depend on many factors: (1) material absorptivity, (2) laser energy, (3) laser power density, (4) pulse duration, (5) welding speed. Localized heat input leads to rapid solidification and fast cooling [46]. Rapid solidification results in finer grain structure and smaller dendrite arm spacing [45].

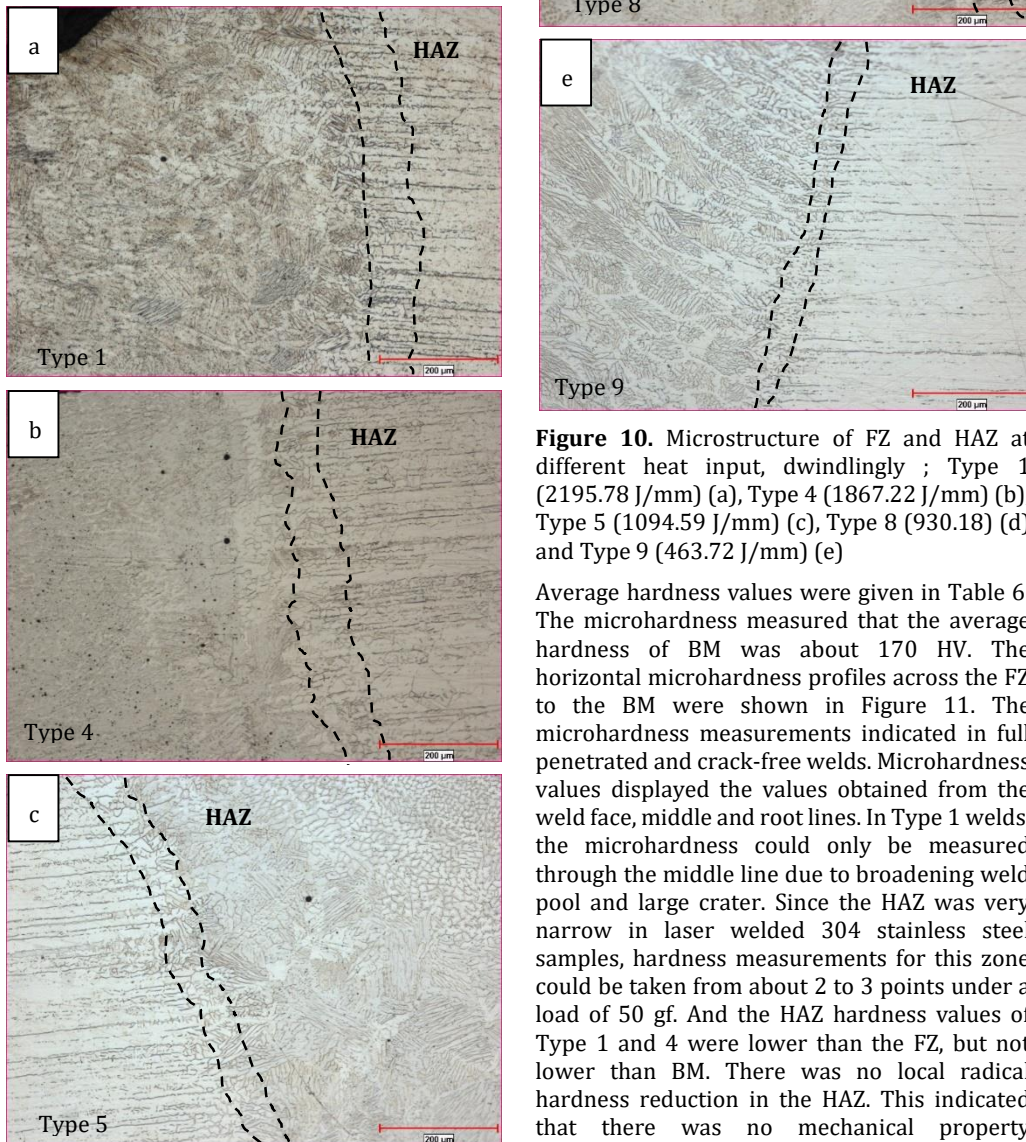


**Figure 10.** Microstructure of FZ and HAZ at different heat input, dwindlingly ; Type 1 (2195.78 J/mm) (a), Type 4 (1867.22 J/mm) (b), Type 5 (1094.59 J/mm) (c), Type 8 (930.18) (d) and Type 9 (463.72 J/mm) (e)

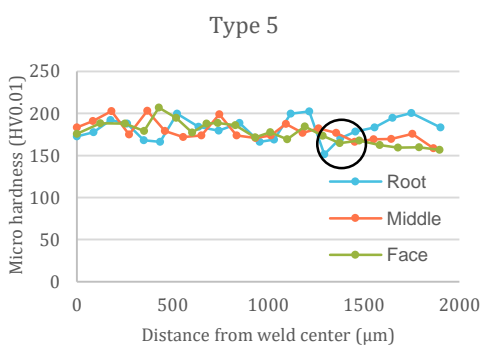
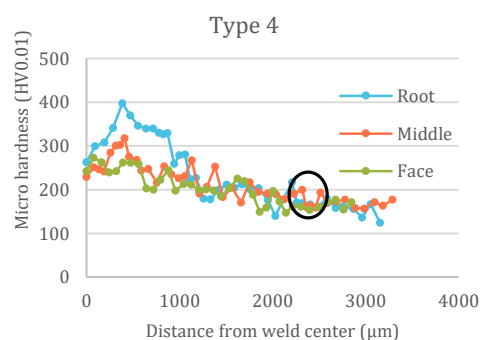
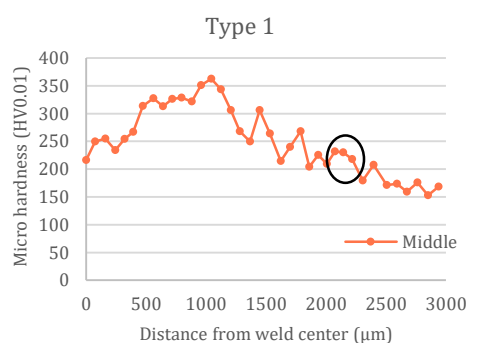
Average hardness values were given in Table 6. The microhardness measured that the average hardness of BM was about 170 HV. The horizontal microhardness profiles across the FZ to the BM were shown in Figure 11. The microhardness measurements indicated in full penetrated and crack-free welds. Microhardness values displayed the values obtained from the weld face, middle and root lines. In Type 1 welds, the microhardness could only be measured through the middle line due to broadening weld pool and large crater. Since the HAZ was very narrow in laser welded 304 stainless steel samples, hardness measurements for this zone could be taken from about 2 to 3 points under a load of 50 gf. And the HAZ hardness values of Type 1 and 4 were lower than the FZ, but not lower than BM. There was no local radical hardness reduction in the HAZ. This indicated that there was no mechanical property weakening due to HAZ. In the Type 4 welds,

some differences were found in the face, middle and root lines of the FZ. For the upper and middle parts, the increase in hardness of the FZ compared to the BM was about 33%. For the lower part, the increase in hardness of the FZ was remarkable compared to the BM and has reached 397 HV, while the BM hardness was around 180 HV. There is an increase of more than 2 times. The microhardness profiles related to the microstructure evolution and also reflected the microstructural properties of welded materials. When the microstructure morphology of Type 4 weld was examined, the presence of equiaxed grain growth was generally dominant in the FZ (Figure 9). The columnar grains formed at the beginning of solidification, i.e. in the root of Type 4 weld. As the solidification continued, the temperature gradient decreased and fine cellular dendrites were formed towards the face and middle. Delta ferrite in weld faces shown with black circle grew in the form fine cellular on the bases austenite. The low cooling rate led to the formation of heterogeneous equiaxed grains on both the face, center and root. At the beginning of solidification, the temperature gradient is high, i.e. in the root of the weld zone, a relatively columnar and very fine-grained growth occurred. The formation of this grain morphology brought about an increase in radically microhardness. Type 1 weldments had large weld pools. The middle line had a trend of increasing and then decreasing in microhardness of Type 1. When the tensile mechanical properties were considered, it was observed that the lowest tensile strength was obtained from Type 1 weldments. Due to the high heat input, heat conduction increased and thus the grain morphology was refined locally. In the Type 1 weld, it was observed that especially the grains consisting of lathy ferrite morphology were thinner (Figure 7c). Therefore, the concentration of delta ferrite is high. Delta ferrite is known to be a harder phase than austenite with FCC crystal [47]. Fine grain size and high  $\delta$ -ferrite content led to high microhardness. This resulted in a relatively increase of average hardness (Table 6).

If the microstructure of the good weld bead morphologies was examined carefully, it could be seen that both Type 5 and Type 8 had extremely narrow HAZ regions.

**Table 6.** Average microhardness of the full penetration welds

Welding condition	Microhardness (HV0.01)			
	Face	Centre	Root	Average
Type 1	-	254.74	-	254.74
Type 4	202.63	214.86	232.95	216.81
Type 5	177.1	179.03	181.67	179.26
Type 8	172.41	164.23	188.76	175.13



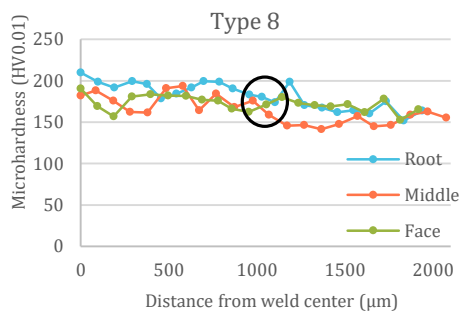


**Figure 11.** Microhardness horizontal profiles across the fusion zone to the base metal

The grain structure of these zones, which was almost adjacent to the fusion line, was fine and the microhardness values were almost uniform in BM, HAZ and FZ. Crater formations are similar and small. According to tensile test results, the difference between Type 5 and 8 was very low, about 30 MPa. This can be explained by the weld bead geometry and the FZ microstructure. Type 5 weld beads are narrower than other full penetrated welds. When compared the FZs (Figure 12), at the beginning and as solidification continues (in root and middle of the weld), the rapid cooling rate and solidification speed limit the development of the side branches and result in the refined dendrite structure. The face of the weld exhibits fine cellular austenite at higher cooling rate. The transition from dendritic to cell is associated with interface stability. It is a result of the degeneration of side branches caused by an increase in temperature gradient during columnar growth [48,49].

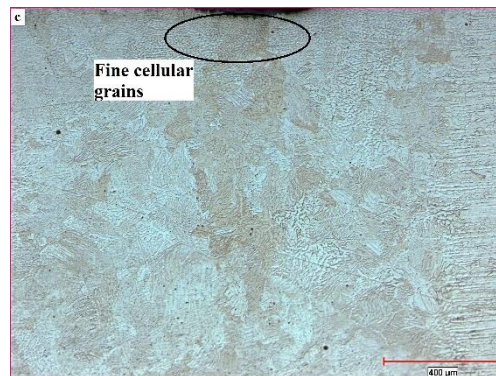
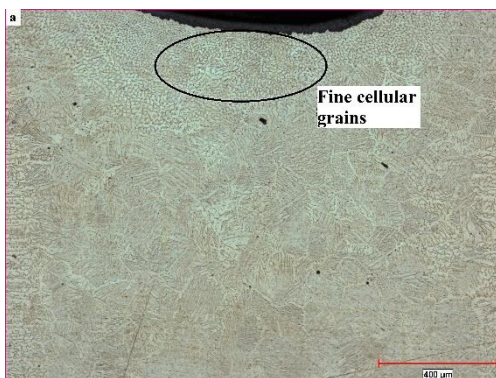


**Figure 12.** Weld microstructure of (a) upper and middle part of Type 5, (b) middle and bottom part of Type 5, (c) upper and middle part of Type 8 and (d) middle and bottom part of Type 8

#### 4. Conclusion

In this study, the effect of heat input, peak power and laser energy on the mechanical and microstructure of the pulsed laser welded 304SS joints are investigated. From the experimental research, we can conclude as follows:

- 1) High-energy pulsed laser welding is a successful joining process for

austenitic stainless steel which has low thermal conductivity.

- 2) This paper showed that increased heat input in high-energy laser beam welding does not lead to complete penetration (Type 2, 3, 6 and 7). The slight increase in peak power for similar heat inputs have increased penetration (Type 1-Type 2 and Type 3-Type 4 and Type 5-Type 6). The heat input is directly proportional to the crater formation.
- 3) It has been found that increasing the heat conduction around the keyhole leads to widening the weld bead. This is related to the heat input. Increasing the heat input leads also to an increase in the HAZ size. The HAZ and FZ size influence the tensile mechanical properties of the joints.
- 4) The welding process used in this study is a high-energy beam process. During laser welding, rapid solidification develops in a very small area. At very low speeds, thermal effect increases, and also overall temperature of the weld metal. The cooling rate is high and therefore the formation of skeletal and lathy delta-ferrite formation is triggered. Laser energy increases the

ferrite network and brings finer ferrites. The coarse ferrite network is formed at a relatively low laser energy and relatively high welding speed. Moreover, in high input, decreasing the laser energy results in equiaxial grain growth.

- 5) Crack formation occurred by reducing the heat input to minimize crater and increasing the peak power to achieve full penetration simultaneously. Increasing the peak power increased the temperature difference between BM and FZ and developed a coarse and columnar grain structure. In addition to the presence of delta-ferrite, a coarse columnar grain morphology facilitates the crack initiation and propagation.
- 6) In Type 5, the best UTS value was obtained as 513.4 MPa. The ductility of this connection is also highest. Type 5 laser welded steel has better strength than BM 304SS. When the weld beam of Type 5 was evaluated morphologically, it was seen that the weld had a very small crater, narrow weld bead and HAZ.

#### Acknowledgment

The authors would like to thank TÜBİTAK (Project Code: 218M631) for providing financial support. They would like to thank Öztaş Demir-Çelik for welding operations.

#### References

- [1] Linjie, Z., Jianxun, Z., Kalaoui, H., Li, H., Wang, Y. 2007. A comparative study of the residual deformation of an automotive gear-case assembly due to deep-penetration high-energy welding. *Journal of Materials Processing Technology*, Cilt. 190(1-3), s. 109-116. DOI:10.1016/j.jmatprotec.2007.03.101
- [2] Kumar, N., Mukherjee, M., Bandyopadhyay, A. 2017. Comparative study of pulsed Nd:YAG laser welding of AISI 304 and AISI 316 stainless steels. *Optics & Laser Technology*, Cilt. 88, s.24-39. DOI:10.1016/j.optlastec.2016.08.018
- [3] Wang, S. C., Wei, P. S. 1992. Energy-Beam redistribution and absorption in a drilling or welding cavity. *Metallurgical Transactions B*, Cilt.23(4),s. 505-511. DOI:10.1007/bf02649669
- [4] Buchwalder, A., Rüttrich, K., Zenker, R., Biermann, H. 2013. *Electron Beam Welding of High Alloy CrMnNi Cast Steels with TRIP/TWIP Effect*. *Advanced Engineering Materials*, Cilt.15(7), s.566-570. DOI:10.1002/adem.201200355
- [5] Bahrami Balajaddeh, M., Naffakh-Moosavy, H. 2019. Pulsed Nd:YAG laser welding of 17-4 PH stainless steel: Microstructure, mechanical properties, and weldability investigation. *Optics & Laser Technology*, Cilt.119, s.105651. DOI:10.1016/j.optlastec.2019.105651
- [6] Wei, X., Ling, X., Zhang, M. 2018. Influence of surface modifications by laser shock processing on the acid chloride stress corrosion cracking susceptibility of AISI 304 stainless steel. *Engineering Failure Analysis*, Cilt. 91, s.165-171. DOI:10.1016/j.engfailanal.2018.04.045
- [7] Zhang, L., Luo, K. Y., Lu, J. Z., Zhang, Y. K., Dai, F. Z., Zhong, J. W. 2011. Effects of laser shock processing with different shocked paths on mechanical properties of laser welded ANSI 304 stainless steel joint. *Materials Science and Engineering: A*, Cilt. 528(13-14), s.4652-4657. DOI:10.1016/j.msea.2011.02.054
- [8] Yang, J., Wang, Y., Li, F., Huang, W., Jing, G., Wang, Z., Zeng, X. 2019. Weldability, microstructure and mechanical properties of laser-welded selective laser melted 304

- stainless steel joints. *Journal of Materials Science & Technology*. DOI:10.1016/j.jmst.2019.04.017
- [9] Mao, K. S., Sun, C., Shiau, C.-H., Yano, K. H., Freyer, P. D., El-Azab, A. A., ... Wharry, J. P. 2020. Role of cavities on deformation-induced martensitic transformation pathways in a laser-welded, neutron irradiated austenitic stainless steel. *Scripta Materialia*, Cilt.178, s.1-6. DOI:10.1016/j.scriptamat.2019.10.037
- [10] Shah, A., Kumar, A., Ramkumar, J. 2018. Analysis of transient thermo-fluidic behavior of melt pool during spot laser welding of 304 stainless-steel. *Journal of Materials Processing Technology*, Cilt.256, s.109-120. DOI:10.1016/j.jmatprotec.2018.02.005
- [11] Geng, Y., Akbari, M., Karimipour, A., Karimi, A., Soleimani, A., Afrand, M. 2019. Effects of the laser parameters on the mechanical properties and microstructure of weld joint in dissimilar pulsed laser welding of AISI 304 and AISI 420. *Infrared Physics & Technology*, Cilt.103, s.103081. DOI:10.1016/j.infrared.2019.103081
- [12] Mukherjee, M., Pal, T. K. 2013. Role of microstructural constituents on surface crack formation during hot rolling of standard and low nickel austenitic stainless steels. *Acta Metallurgica Sinica (English Letters)*, Cilt.26(2), s.206-216. DOI:10.1007/s40195-012-0200-7
- [13] Zhang, L., Lu, J. Z., Luo, K. Y., Feng, A. X., Dai, F. Z., Zhong, J. S., ... Zhang, Y. K. 2013. Residual stress, micro-hardness and tensile properties of ANSI 304 stainless steel thick sheet by fiber laser welding. *Materials Science and Engineering: A*, Cilt. 561, s.136-144. DOI:10.1016/j.msea.2012.11.001
- [14] Al-Roubaiy A. 2016. Characterization of the nugget zone between Aluminum and 304 Stainless Steel Laser Welded. *Advances in Natural and Applied Sciences*. DOI:10(12),38-49.
- [15] Zhang, M., Chen, G., Zhou, Y., Liao, S. 2014. Optimization of deep penetration laser welding of thick stainless steel with a 10kW fiber laser. *Materials & Design*, Cilt. 53, s.568-576. DOI:10.1016/j.matdes.2013.06.066
- [16] Hafez, K. M., Katayama, S. 2009. Fiber laser welding of AISI 304 stainless steel plates. *Quarterly Journal Of The Japan Welding Society*. Cilt.27(2), s.69-73.
- [17] Cui C.Y. , Cui X.G. , Ren X.D. , Liu T.T. , J.D.Hu Wang Y.M. 2013. Microstructure and microhardness of bre laser butt welded joint of stainless steel plates. *Mater. Design*. Cilt.49,s. 761-765.
- [18] Balasubramanian K.R., Siva Shanmugam N., Buvanashakaran G., Sankaranarayanan K. 2008. Numerical and experimental investigation of laser beam welding of AISI 304 stainless steel sheet. *Adv. Produc. Engineer Manag*. Cilt.3(2), s.93-105.
- [19] Taskin, M., Elazig, U. C., Turkmen, M. 2011. X-ray tests of AISI 430 and 304 stainless steels and AISI 1010 low carbon steel welded by CO2 laser beam welding. *Materials Testing*, Cilt. 53(11-12),s. 741-747. DOI:10.3139/120.110283
- [20] Petretis, Br , Balciuniene, M. 2005. Peculiarities of laser welding of metals. *Lithuanian J. Phys.* Cilt.45(1) , s.59-69.
- [21] Wang, X-N., Sun, Q., Zheng, Z. Di, H-S. 2017. Microstructure and fracture behavior of laser welded joints of DP steels with different heat inputs. *Mat. Sci. Eng. A-Struct* , Cilt.699,s.18-25.
- [22] Akman, E., Demir, A., Canel, T., Sinmazçelik, T. 2009. Laser welding of Ti6Al4V titanium alloys. *Journal of materials processing technology*, Cilt.209(8), s.3705-3713. DOI:10.1016/j.jmatprotec.2008.08.026
- [23] Saha, P., Datta, S., Raza, M. S., Pratihari, D. K. 2019. Effects of heat input on weld-bead geometry, surface chemical composition, corrosion behavior and thermal properties of fiber laser-welded nitinol shape memory alloy. *Journal of Materials Engineering and Performance*, Cilt.28(5), s.2754-2763. DOI:10.1007/s11665-019-04077-0
- [24] Li, R., Li, Z., Zhu, Y., Rong, L. 2011. A comparative study of laser beam welding and laser-MIG hybrid welding of Ti-Al-Zr-Fe titanium alloy. *Materials Science and Engineering: A*, Cilt.528(3),s. 1138-1142. DOI:10.1016/j.msea.2010.09.084
- [25] Chatterjee, S., Sahoo, S. K., Swain, B., Mahapatra, S. S., Roy, T. 2020. Quality characterization of dissimilar laser welded joints of Ti6Al4V with AISI 304 by using copper deposition technique. *The International Journal of Advanced Manufacturing Technology*. DOI:10.1007/s00170-020-04935-5
- [26] Anawa, E. M., Olabi, A. G. 2008. Control of welding residual stress for dissimilar laser welded materials. *Journal of Materials Processing Technology*, Cilt.204(1-3), s.22-33. DOI:10.1016/j.jmatprotec.2008.03.047
- [27] Kangazian, J., Shamanian, M. 2016. Multiresponse Optimization of Pulsed-Current Gas Tungsten Arc Welding (PCGTAW) for AISI 304 Stainless Steel to St 52 Steel Dissimilar Welds. *Metallography, Microstructure, and Analysis*, Cilt. 5(3), s.241-250. DOI:10.1007/s13632-016-0277-x
- [28] Bahrami Balajaddeh, M., Naffakh-Moosavy, H. 2019. Pulsed Nd:YAG laser welding of 17-4 PH stainless steel: Microstructure, mechanical properties, and weldability investigation. *Optik Laser Technology*, Cilt. 119,s.105651.
- [29] Bilmes, P., Gonzalez, A., Llorente, C., Solari, M. 1996. Effect of ferrite solidification morphology of austenitic stainless steel weld metal on properties of welded joints. *Welding International*, Cilt.10(10), s.797-808. DOI:10.1080/09507119609549091
- [30] Chen, B., Flewitt, P. E. J., & Smith, D. J. 2010. Microstructural sensitivity of 316H austenitic stainless steel: Residual stress relaxation and

- grain boundary fracture. *Materials Science and Engineering: A*, 527(27-28), 7387-7399. DOI:10.1016/j.msea.2010.08.010
- [31] Sheikhi, M., Malek Ghaini, F., Torkamany, M. J., Sabbaghzadeh, J. 2009. Characterisation of solidification cracking in pulsed Nd:YAG laser welding of 2024 aluminium alloy. *Science and Technology of Welding and Joining*, Cilt.14(2), s.161-165. DOI:10.1179/136217108x386554
- [32] Katayama, S. 2000. Solidification phenomena of weld metals (1st report). Characteristic solidification morphologies, microstructures and solidification theory. *Welding International*, Cilt.14(12),s. 939-951. DOI:10.1080/09507110009549297
- [33] Sheikhi, M., Malek Ghaini, F., Torkamany, M. J., Sabbaghzadeh, J. 2009. Characterisation of solidification cracking in pulsed Nd:YAG laser welding of 2024 aluminium alloy. *Science and Technology of Welding and Joining*, Cilt.14(2), s.161-165. DOI:10.1179/136217108x386554
- [34] Kim, S. K., Lee, Y. D., Hansson, K., Fredriksson, H. 2002. Influence of Cooling Rate on the Hot Cracking Formation of Nickel Rich Alloys. *ISIJ International*, Cilt.42(5), s.512-519. DOI:10.2355/isijinternational.42.512
- [35] Fabbro, R. 2019. Scaling laws for the laser welding process in keyhole mode. *Journal of Materials Processing Technology*, Cilt.264, s.346-351. DOI:10.1016/j.jmatprotec.2018.09.027
- [36] Matsunawa, A., Mizutani, M., Katayama, S., Seto, N. 2003. Porosity formation mechanism and its prevention in laser welding. *Welding International*, Cilt.17(6), s.431-437. DOI:10.1533/wint.2003.3138
- [37] Matsunawa, A. 2001. Problems and solutions in deep penetration laser welding. *Science and Technology of Welding and Joining*, Cilt.6(6), s.351-354. DOI:10.1179/stw.2001.6.6.351
- [38] Dawes, C.T.1992. *Laser Welding A Practical Guide*, 1st edition Woodhead Publishing.
- [39] Saravanan, S., Sivagurumanikandan, N., Raghukandan, K. 2019. Effect of heat input on microstructure and mechanical properties of Nd: YAG laser welded super duplex stainless steel-Numerical and experimental approach. *Optik*. DOI:10.1016/j.ijleo.2019.03.145
- [40] Farabi, N., Chen, D. L., Zhou, Y. 2011. Microstructure and mechanical properties of laser welded dissimilar DP600/DP980 dual-phase steel joints. *Journal of Alloys and Compounds*, Cilt.509(3),s. 982-989. DOI:10.1016/j.jallcom.2010.08.158
- [41] Kumar, S., Shahi, A. S. 2011. Effect of heat input on the microstructure and mechanical properties of gas tungsten arc welded AISI 304 stainless steel joints. *Materials & Design*, Cilt.32(6),s. 3617-3623. DOI:10.1016/j.matdes.2011.02.017
- [42] Wollin, P., Gooch, T.G.1995. *Welding processes for stainless Steels*. *Welding World Journal*. Cilt.36,s.75-82.
- [43] Benyounis, K. Y., Olabi, A. G., Hashmi, M. S. J. 2008. Multi-response optimization of CO2 laser-welding process of austenitic stainless steel. *Optics & Laser Technology*,Cilt. 40(1), s.76-87. DOI:10.1016/j.optlastec.2007.03.009
- [44] Osoba, L. O., Ojo, O. A. 2012. Influence of laser welding heat input on HAZ cracking in newly developed Haynes 282 superalloy. *Materials Science and Technology*, Cilt.28(4), s.431-436. DOI:10.1179/1743284711y.0000000078
- [45] Zacharia, T., David, S. A., Vitek, J. M., Debroy, T. 1989. Heat transfer during Nd: Yag pulsed laser welding and its effect on solidification structure of austenitic stainless steels. *Metallurgical Transactions A*, Cilt.20(5), s.957-967. DOI:10.1007/bf02651661
- [46] Vrancken, B., Thijs, L. , Kruth, J.P.2012. Van Humbeeck J.Heat treatment of Ti6Al4V produced by Selective Laser Melting:Microstructure and mechanical properties.*J. Alloy. Compd*.Cilt.541,s.177.
- [47] Chen, R., Jiang, P., Shao, X., Mi, G., Wang, C. 2017. Analysis of crack tip transformation zone in austenitic stainless steel laser-MIG hybrid welded joint. *Materials Characterization*,Cilt. 132, s.260-268. DOI:10.1016/j.matchar.2017.08.022
- [48] Hao, C., Chun-xu, P. 2003. Microstructure and fractural morphology of cobalt-based alloy laser cladding. *Journal of Wuhan University of Technology-Mater. Sci. Ed.*, Cilt.18(3), s.30-32. DOI:10.1007/bf02838452
- [49] Fu, J. W., Yang, Y. S., Guo, J. J., Tong, W. H. 2008. Effect of cooling rate on solidification microstructures in AISI 304 stainless steel. *Materials Science and Technology*, Cilt.24(8),s. 941-944. DOI:10.1179/174328408x295962